OPEN ACCESS

ACTA METALLURGICA SLOVACA

2026, VOL. 32, NO. 3, 241-250

SCICELL

RESEARCH PAPER

Thermodynamic mechanism of non-metallic inclusions modification in recycled low-alloyed cast steel using $CaCO_3$–$CaSiO_3$ composite mineral fluxes

Nozimjon Kholmirzaev[1], Nodir Turakhodjaev[1], Jamshidbek Khasanov[2], Abdujalol Bektemirov[3], Nosir Saidmakhamadov[4], Zokirjon Nurdinov[1], Shovkat Tursunov[5], Shakhzodjon Turdiev[6], Rustam Parpiev[1], Farkhad Maksumov[1], Dilshod Sartibayev[1], Kamoliddin Khasanov[7]

[1]Department of Metal Technologies, Tashkent State Technical University, 100095 Tashkent, Uzbekistan
[2]Department of Mechanical Engineering, Andijan State Technical Institute, 170100, Andijan, Uzbekistan
[3]Laboratory of Mechanical Engineering and Materials Science, Uzbek-Japan Innovation Center of Youth, 100095 Tashkent, Uzbekistan
[4]Department of Mechanical Engineering, Namangan State Technical University, 160100, Namangan, Uzbekistan
[5]Department of Mechanical Engineering, Fergana State Technical University, 150100, Fergana, Uzbekistan
[6]Department of Materials Science and Mechanical Engineering, Tashkent State Transport University, 100001, Tashkent, Uzbekistan
[7]Faculty of Engineering, Kimyo International University in Tashkent Branch Samarkand, Samarkand 140100, Uzbekistan

*Corresponding author: nozimjonxolmirzayev@gmail.com , tel.: +998911722233, Department of Metal Technologies, Faculty of Mechanical Engineering, Tashkent State Technical University named after Islam Karimov, 100095 Tashkent, Uzbekistan

Received: 11.08.2026
Accepted: 23.08.2026

ABSTRACT

In this study, the effects of $CaCO_3$–$CaSiO_3$ mineral fluxes on the evolution of non-metallic inclusions and phase transformations during the remelting of SCMnCr3 cast steel produced from secondary metal scrap were investigated. To determine the optimum slag composition, four fluxes containing 50–80 wt.% $CaCO_3$ were evaluated. The evolution of the microstructure was characterized using optical microscopy, scanning electron microscopy (SEM), energy-dispersive X-ray spectroscopy (EDS), elemental mapping, and X-ray diffraction (XRD). Thermodynamic analysis was performed to explain the mechanisms responsible for inclusion transformation. The obtained results showed that the flux consisting of 70 wt.% $CaCO_3$ and 30 wt.% $CaSiO_3$ (F3) produced the cleanest microstructure. Under these conditions, the amount of large and irregularly shaped inclusions was significantly reduced, while they were replaced by fine spherical inclusions uniformly distributed throughout the matrix. SEM–EDS and elemental mapping confirmed the uniform distribution of Fe, Mn, Cr, Si, Ca, and O within the investigated regions. This indicates effective inclusion modification and stable interaction between the slag and the molten metal. XRD analysis confirmed the formation of thermodynamically stable calcium silicate phases. The addition of an excessive amount of $CaCO_3$ (80 wt.%) resulted in excessive CO_2 gas evolution during its decomposition. This intensified secondary oxidation and reduced the metallurgical cleanliness of the steel.

Keywords: SCMnCr3 cast steel, composite mineral flux, slag, non-metallic inclusions, Gibbs free energy, X-ray diffraction (XRD)

INTRODUCTION

Steel alloys are among the most widely used engineering materials owing to their high strength, good ductility, excellent weldability, and relatively low production cost. They play a vital role in construction, transportation, machinery manufacturing, energy, and numerous other industrial sectors. Over the past decades, the increasing demand for sustainable manufacturing technologies has significantly expanded the use of secondary steel produced from recycled metal scrap [1,2]. Steel recycling reduces energy consumption, lowers greenhouse gas emissions, and decreases the demand for natural iron ore resources [3,4]. Consequently, secondary steel production has become one of the major development directions in modern metallurgy.

However, the remelting of secondary steel is associated with several metallurgical challenges that directly affect the quality of the final product. One of the most important problems is the development of non-metallic inclusions during melting and solidification. These inclusions are the main factors limiting the mechanical properties, fatigue resistance, corrosion resistance and service life of steel products. Even very small amounts of oxide and sulfide inclusions can act as stress concentration sites, promoting crack initiation and propagation under cyclic loading conditions [5–7].

The sources of non-metallic inclusions are diverse. The primary inclusions are formed during the steelmaking from the deoxidation reactions, while the secondary inclusions are generated during remelting due to oxidation, slag–metal reactions, refractory degradation or gas–metal interactions [8–11]. During secondary remelting, existing inclusions may either remain within the metal matrix or undergo modification depending on the thermodynamic conditions of the slag system [12,13]. Therefore, controlling the evolution of non-metallic inclusions during remelting is one of the most important objectives of secondary metallurgy. The inclusion removal and modification are mainly achieved through physicochemical interactions between molten steel and slag [14,15]. Slag plays an important role in the metallurgical process, such as protecting the molten metal from atmospheric oxidation, fixing detrimental impurities, controlling the transfer of sulfur and phosphorus, and encouraging the flotation of non-metallic inclusions into the slag phase [16–19]. Therefore, the cleanliness of steel depends to a large extent on the chemical composition and physicochemical properties of the slag.

The formation, composition, size, morphology, and distribution of non-metallic inclusions directly influence the mechanical properties, fatigue resistance, fracture toughness, corrosion resistance, and service reliability of steel products. Consequently, steel cleanliness has become one of the key quality indicators in the production of high-performance structural steels. Large and irregularly shaped inclusions serve as stress concentration sites, accelerating crack initiation and propagation, and causing nozzle clogging during the continuous casting process, thereby reducing process stability and product quality. Therefore, investigating the formation and evolution of non-metallic inclusions has become one of the most important research directions in modern steelmaking [20–22].

Inclusions are formed during steelmaking through deoxidation reactions, slag–metal interactions, refractory degradation, secondary oxidation, and solidification processes. Their composition continuously evolves throughout molten steel refining and casting. Industrial observations have shown that the initially formed aluminum oxide (Al_2O_3) inclusions are eventually transformed into spinel and calcium-containing inclusions through interactions with dissolved Mg and Ca originating from the slag and refractory materials. This continuous evolution determines not only the morphology of the inclusions but also their

flotation behavior and ultimate removal efficiency. Thermodynamic transformations govern the evolution of inclusions, as confirmed by numerous studies [23–25].

Deng and Zhu [24] showed that the evolution of inclusions in Al-deoxidized steels during secondary refining follows the sequence of $Al_2O_3 \rightarrow MgO - Al_2O_3 \rightarrow$ spinel $\rightarrow CaO–MgO–Al_2O_3 \rightarrow$ spherical calcium aluminate inclusions. Their industrial observations and thermodynamic calculations confirmed that dissolved Mg forms earlier than dissolved Ca because the thermodynamic stability of MgO is lower than that of CaO. Subsequently, Ca replaces Mg in the spinel structure thus favoring the formation of low melting calcium aluminate phases.

Furthermore, industrial tracer tests have shown that the origin of inclusions is considerably more complex than previously assumed. Tang et al. [23] indicated that the fine inclusions are mainly generated during the deoxidation process, and the large inclusions are mainly formed by the ladle and mold slags entraining into the molten steel. They also confirmed that calcium treatment is beneficial to convert alumina inclusions into liquid calcium aluminates, which improves the cleanliness of steel and reduces inclusion-related defects.

Instead of the conventional calcium wire treatment, refining slag compositions are being optimized in more and more recent studies. High basicity slags can simultaneously realize deoxidation, desulfurization, inclusion modification and inclusion flotation. Laboratory investigations performed on HSLA steels have shown that an increase in the basicity of slags leads to the formation of low-melting inclusions in the $CaO - MgO - Al_2O_3 - SiO_2$ system and to the decrease of large and irregular oxide particles [26,27].

Similarly, the effect of slag basicity on the inclusion evolution was studied by Zhan et al. [22] in 15-5PH stainless steel. The results indicated that the enhancement of slag basicity significantly decreased the average size of inclusions and increased their absorption by the refining slag. Thermodynamic analysis indicated that the increase in slag basicity led to the variation of oxide stability and transformation sequence of $Al_2O_3 \rightarrow MgAl_2O_3 \rightarrow MgO$, and enhanced the cleanliness of steel. Optimization of refining slag composition has also been successfully applied in the production of alloyed structural steels.

According to the results of Xu et al. [28], the optimized high-basicity refining slag can reduce the size and number density of non-metallic inclusions in 38CrMoAl steel and avoid nozzle clogging in industrial production. Their results demonstrated that, if properly designed, slag systems can be a partial substitute for conventional calcium treatment, by providing adequate calcium transfer from the slag to the molten steel.

Thermodynamic modeling has been developed as an important tool in addition to slag composition to predict inclusion formation and transformation. Cao et al. [29] calculated the equilibrium relationships for the deoxidation of GCr15 bearing steel by the FactSage software. They showed that the thermodynamic analysis can be used to predict the evolution of inclusions under different alloying conditions. Recent numerical modeling studies showed that the flotation efficiency of oxide inclusions is highly dependent on the slag viscosity, the interfacial tension and the wettability of inclusions. The above results emphasize the necessity of accounting simultaneously for the thermodynamic and kinetic factors in the design of refining slags [30].

The extensive use of SEM-EDS, elemental mapping, X-ray diffraction (XRD) and thermodynamic modelling has significantly improved the understanding of the evolution of inclusions. The recent studies have been devoted not only to the determination of the inclusion composition, but also to the evaluation of their number density, particle size distribution, equivalent circular diameter and their statistical evolution during the refining process. These quantitative characterization methods provide a more comprehensive assessment of steel cleanliness and help establish direct relationships between slag chemistry and inclusion behavior [31–34].

Although substantial progress has been achieved in understanding inclusion evolution in Al-deoxidized steels, stainless steels, bearing steels, HSLA steels, and pipeline steels, most previous studies have focused on conventional $CaO - Al_2O_3$ based refining slags, calcium wire treatment, or industrial ladle refining processes. In contrast, the application of $CaCO_3 - CaSiO_3$ composite mineral fluxes for the remelting of recycled cast steels have received very limited attention. In particular, the thermodynamic effects of varying the $CaCO_3/CaSiO_3$ ratio on inclusion modification, phase evolution, and microstructural refinement in recycled SCMnCr3 cast steel have not yet been sufficiently investigated [35–38].

In the present study, the evolution of non-metallic inclusions during the remelting of recycled SCMnCr3 cast steel using composite mineral fluxes with different $CaCO_3/CaSiO_3$ ratios were investigated. Optical microscopy, SEM, EDS, elemental mapping, XRD analysis, and thermodynamic calculations were jointly employed to elucidate the relationships among slag composition, inclusion evolution, and steel cleanliness. The obtained results provide a theoretical and experimental basis for optimizing environmentally friendly mineral fluxes for secondary steel recycling and improving the metallurgical quality of recycled cast steels.

MATERIAL AND METHODS

Experimental materials

To ensure identical experimental conditions, each melting experiment was carried out in a 10 kg electric induction furnace using a 6 kg steel charge. Maintaining a constant metal mass enabled the direct comparison of slag formation, the evolution of non-metallic inclusions, and thermodynamic parameters for different flux compositions. For this study, low-alloy SCMnCr3 steel produced by the remelting of secondary metal scrap was selected as the experimental material.

Table 1 Chemical composition of the sample steel (wt.%)

Elements					
C	Mn	Si	P	S	Cr
0.39	1.05	0.82	0.031	0.026	0.89

Preparation of the composite mineral flux. The flux used in this study consisted of chemically pure calcium carbonate ($CaCO_3$) and calcium silicate ($CaSiO_3$). These minerals perform complementary functions during the steel remelting process. Calcium carbonate serves as the source of basic oxides. At high temperatures, $CaCO_3$ decomposes according to the following reaction:

$$CaCO_3 \rightarrow CaO + CO_2 \quad (1.)$$

The resulting CaO increases the basicity of the slag and promotes the absorption of acidic oxide inclusions. At the same time, it enhances the inclusion modification reactions. During the process, the released CO_2 gas intensifies bath stirring and improves mass transfer between the molten steel and the slag. Calcium silicate stabilizes the slag structure, lowers its melting temperature, and controls its viscosity. Another important function is the improvement of slag fluidity. The optimum slag viscosity is beneficial for flotation of non-metallic inclusions into the slag phase and prevention of excessive foaming. Selected minerals were dried in a laboratory drying oven at 120 ℃ for 2 h to remove absorbed moisture before mixing. This was done to reduce the production of hydrogen and to prevent further gas evolution during melting.

The dried powders were weighed using an analytical balance with an accuracy of ±0.001 g. The two components were mechanically mixed for approximately 20 min to ensure their uniform distribution. Four different flux compositions were prepared while maintaining a constant total flux mass for each experiment.

Table 2 Composition of the investigated composite mineral fluxes (wt.%)

Flux	F1	F2	F3	F4
$CaCO_3$	50	60	70	80
$CaSiO_3$	50	40	30	20

The total charge mass was fixed at 6 kg for all experiments. A total of 0.05 kg (50 g) of the $CaCO_3 - CaSiO_3$ composite flux was added to each charge, corresponding to approximately 0.83 wt.% of the initial charge mass. The $CaCO_3/CaSiO_3$ ratios of F1–F4 were calculated based on this total flux mass.

The mass of the resulting slag was approximately 0.72 kg per 6 kg charge, corresponding to approximately 12 wt.% relative to the initial charge mass.

Each flux composition was investigated in a separate melting experiment. Samples were taken at different stages of the melting and casting process, i.e. at the furnace stage, the casting stage and the final stage. For each flux composition three samples were prepared, giving a total of 12 experimental samples for the four flux compositions studied.

Experimental procedure. The melting experiments were carried out in a laboratory medium-frequency induction furnace with a capacity of 10 kg. The furnace was equipped with an alumina (Al_2O_3) crucible capable of operating at temperatures up to 1700 ℃. The ready steel charge was put into the crucible and heated to the full melting. The melting temperature was kept in the range of 1550-1600 ℃. The temperature was recorded continuously with a calibrated optical

pyrometer (accuracy ± 5 ℃). After complete melting of the steel, the pre-prepared composite mineral flux was gradually added onto the surface of the molten steel. The flux was added slowly to prevent excessive local gas evolution caused by the rapid decomposition of $CaCO_3$ and to ensure its uniform distribution. After addition of the flux, the molten steel was kept under isothermal conditions for about 10 min to ensure adequate interaction between the molten metal and slag phases. During the holding time several physicochemical processes took place simultaneous. These included the decomposition of calcium carbonate ($CaCO_3$) and the formation of calcium oxide (CaO), which increased the slag basicity and thereby enhanced its ability to absorb oxide inclusions. At the same time, inclusion modification occurred, followed by the flotation of inclusions into the slag layer. In addition, calcium silicate and calcium aluminate phases were formed, which play a decisive role in determining the composition and properties of the slag. After completion of the refining stage, the molten steel was poured into preheated sand-clay molds and allowed to solidify under atmospheric conditions. To ensure statistical reliability, five independent samples were prepared for each experimental condition. Each sample was cleaned of the sand-clay mold mixture and machined to standard specimen dimensions in the presence of a coolant after solidification [39–41].

Metallographic investigations

Samples for the metallographic investigations were cast into pre-prepared molds. The specimens were first ground using SiC abrasive papers with grit sizes ranging from 320 to 2500. They were then polished with diamond suspension until a mirror-like surface was obtained. The polished specimens were etched in 2% Nital solution for approximately 10–15 s to reveal the ferrite–pearlite microstructure. Optical metallographic observations were performed using an optical microscope at magnifications of ×20, ×50, ×100, ×200, and ×500. For each specimen, the number of non-metallic inclusions per 1 mm², the average inclusion diameter, inclusion morphology and distribution, ferrite grain size, and the volume fraction of pearlite were evaluated.

X-ray diffraction (XRD) analysis

The crystalline phases formed during the remelting process were identified by X-ray diffraction (XRD) analysis of the slag and steel samples, and the effect of the composite mineral flux composition on slag chemistry was evaluated. X-ray diffraction is one of the most reliable methods for phase identification, as each crystalline phase has a unique diffraction pattern characteristic of its crystal lattice. Diffraction analysis was performed by an X-ray diffractometer with a Cu–Kα radiation source with a wavelength of λ = 1.5406 Å. The scanning was performed from 10° to 90° (2θ) with a step size of 0.02° and a scanning rate of 2° m. These experimental conditions were selected to provide sufficient resolution for distinguishing calcium silicate, calcium aluminate, iron oxide, and silicon dioxide phases. Phase identification was performed by comparing the obtained diffraction peaks with the standard diffraction patterns in the International Centre for Diffraction Data (ICDD PDF-4+) database. The principal crystalline phases expected to be identified in the slag system included $CaO, SiO_2, FeO, CaSiO_3, Ca_2SiO_4, CaAl_2O_4$ and $CaAl_4O_7$. Graphical abstract of the research methodology, **Fig. 1**, presents the experimental study

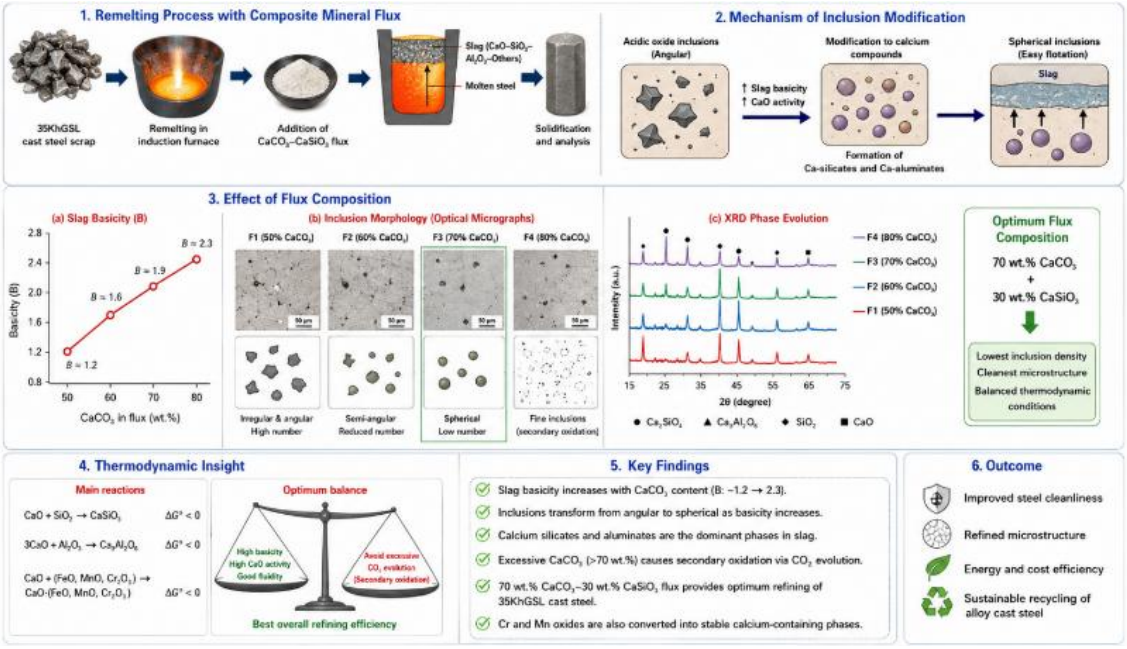

Fig. 1 Graphical abstract of the research methodology

Thermodynamic analysis

Classical thermodynamic principles were employed to explain the physicochemical processes occurring in the slag–metal system during the remelting of secondary metals. Within the scope of this study, slag basicity, the mole fractions of oxides, thermodynamic activity, Gibbs free energy, and the formation of equilibrium phases were analyzed. These factors were used to explain the mechanism of modification and removal of non-metallic inclusions during the remelting process. Upon heating, calcium carbonate decomposes according to Reaction (1).

The decomposition temperature of calcium carbonate is approximately 840–900 ℃. Since the melting temperature in the present study was 1550–1600 ℃, the complete decomposition of $CaCO_3$ was assumed. CaO is the principal basic oxide in the slag system. The released CO_2 simultaneously enhances bath stirring and improves mass transfer between the molten steel and the slag [42]. However, excessive CO_2 evolution may also intensify the oxidation of the molten steel.

Slag basicity. Slag basicity is one of the most important physicochemical properties of metallurgical slag. In the present study, the slag basicity was calculated using the following equation:

$$B = \frac{CaO}{SiO_2} \qquad (2.)$$

where: CaO – the mass fraction of the basic oxide;
SiO_2 – the mass fraction of the acidic oxide.

Therefore, the actual CaO content in the slag was determined based on stoichiometric calculations.

Molar masses: M_{CaCO_3} = 100.09 g/mol, M_{CaO} = 56.08 g/mol.

Thus, the decomposition of 1 kg of $CaCO_3$ produces approximately 0.56 kg of CaO. The calculated CaO content was used to determine the slag basicity.

Calculation of mole fractions. Thermodynamic reactions depend on the number of moles of the substances rather than their mass percentages. Therefore, the mass fractions of the oxides were converted into mole fractions. The number of moles of each oxide was calculated using the following equation:

$$n_i = \frac{w_i}{M_i} \quad (3.)$$

where: w_i – the mass of the oxide;
M_i – the molar mass of the oxide.

The total number of moles is:

$$n_{total} = \sum n_i \quad (4.)$$

Each component's mole fraction is given by:

$$X_i = \frac{n_i}{\sum n_i} \quad (5.)$$

These mole fractions were subsequently used in the calculation of thermodynamic activity.

Calculation of thermodynamic activity. Industrial slags are multicomponent and non-ideal solutions. Therefore, the effective concentration of each oxide is not equal to its simple mole fraction. The thermodynamic activity of an oxide is determined by the following expression:

$$a_i = \gamma_i X_i \quad (6.)$$

where: a_i – the thermodynamic activity;
γ_i – the activity coefficient;
X_i – the mole fraction.

The activity coefficients were calculated based on thermodynamic data reported in the literature for the $CaO - SiO_2 - Al_2O_3$ system at steelmaking temperatures. An increase in the activity of CaO enhances inclusion modification, whereas an increase in the activity of CO_2 may intensify secondary oxidation.

Gibbs free energy. Gibbs free energy was used to evaluate the spontaneity of chemical reactions.

The fundamental equation:

$$\Delta G = \Delta G^0 + RT \ln Q \quad (7.)$$

where: R = 8.314 J/mol·K is the universal gas constant;
T – the absolute temperature (K);
Q – the reaction quotient.

Major metallurgical reactions. The following principal reactions were evaluated in the thermodynamic analysis.

Formation of calcium silicate: $CaO + SiO_2 \rightarrow CaSiO_3$ (8.)
Formation of calcium aluminate: $CaO + Al_2O_3 \rightarrow CaAl_2O_4$ (9.)
Desulfurization: $CaO + FeS \rightarrow CaS + FeO$ (10.)
Secondary oxidation: $Fe + CO_2 \rightarrow FeO + CO$ (11.)

Each reaction was evaluated based on the Gibbs free energy and the thermodynamic activities of the oxides. An Ellingham diagram was used to interpret the thermodynamic stability of the oxide phases. The diagram illustrates the temperature dependence of Gibbs free energy:

$$\Delta G = f(T) \quad (12.)$$

Oxides located in the lower part of the diagram possess higher thermodynamic stability. Calcium has a rather high affinity to the acidic oxides, as the Gibbs free energy of CaO is much lower than that of FeO. Therefore, the thermodynamic explanations of the transformation of oxide inclusions into calcium-containing compounds were based on the Ellingham diagram.

$CaO - SiO_2$ phase diagram. The evolution of slag phases of research alloy was analyzed using the $CaO - SiO_2$ binary phase diagram, **Fig. 2**. This diagram includes the stable phases $CaSiO_3$, Ca_2SiO_4 liquid slag, and excess CaO. The formation of low-melting calcium silicate phases reduces slag viscosity and facilitates the flotation of non-metallic inclusions into the slag.

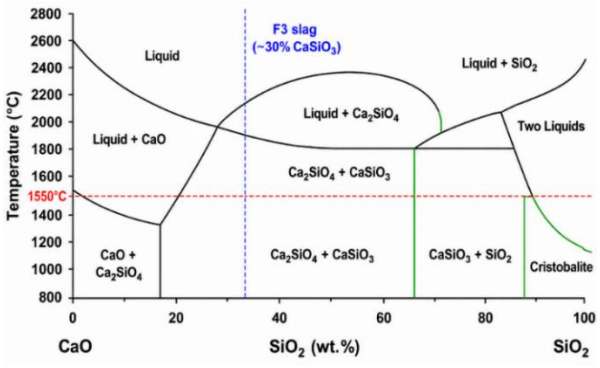

Fig. 2 $CaO - SiO_2$ phase diagram

RESULTS AND DISCUSSION

Metallographic analysis using optical microscopy

The microstructural evolution of remelted SCMnCr3 low-alloy cast steel under the influence of different compositions of the $CaCO_3 - CaSiO_3$ composite flux was investigated by optical metallographic observations. After etching with a 2% Nital solution, microstructural images were obtained at magnifications ranging from ×20 to ×500. Particular attention was paid to the morphology, size, and spatial distribution of non-metallic inclusions, as well as to the effect of slag chemistry on the ferrite–pearlite matrix.

Compared with plain carbon steels, SCMnCr3 contains chromium (Cr), manganese (Mn), and silicon (Si), which significantly influence oxidation reactions and phase transformations during the remelting process. Manganese participates in deoxidation reactions and may form manganese oxide or complex manganese–silicate inclusions. Chromium improves oxidation resistance and promotes the formation of stable chromium-containing oxide phases. Silicon influences slag chemistry through the formation of silicate phases [43–45]. Therefore, the interaction between the molten steel and the $CaCO_3 - CaSiO_3$ slag is considerably more complex than that in plain carbon steels and should be analyzed jointly from metallographic and thermodynamic perspectives.

The optical microstructures of SCMnCr3 cast steel remelted using different compositions of the $CaCO_3 - CaSiO_3$ composite flux is presented in **Fig. 3**.

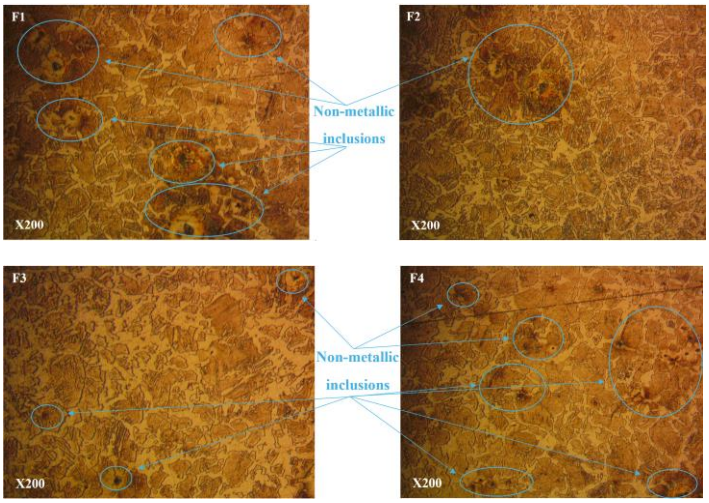

Fig. 3 Microstructures of the samples produced using different flux compositions

A gradual change in the morphology of non-metallic inclusions was observed with increasing $CaCO_3$ content, confirming that the slag composition significantly influences inclusion modification during the remelting process. The

microstructural changes indicate that the refining efficiency is governed not only by slag basicity but also by the balance between calcium activity and slag fluidity. The F1 flux (50 wt.% $CaCO_3$–50 wt.% $CaSiO_3$) produced a ferrite–pearlite microstructure containing numerous large, angular non-metallic inclusions distributed throughout the steel matrix. Such inclusions are characteristic of oxide particles that have undergone only partial modification during the remelting process. Their irregular morphology indicates that the amount of CaO generated by the decomposition of $CaCO_3$ was insufficient to ensure significant interaction between the acidic oxide inclusions and the refining slag. As a result, a large proportion of the primary oxide inclusions remained trapped within the steel matrix instead of being transferred into the slag phase.

These results are in good agreement with the inclusion evolution mechanism proposed by Deng and Zhu [24,25]. They reported that insufficient calcium activity prevents the transformation of alumina-rich inclusions into low-melting calcium-containing phases. Tang et al. [23] also obtained similar results, showing that large angular inclusions are generally associated with low refining efficiency and incomplete absorption of inclusions by the slag. The low basicity of the F1 slag limited inclusion modification and flotation, resulting in the lowest metallurgical cleanliness among the investigated compositions.

Increasing the $CaCO_3$ content to 60 wt.% (F2) significantly improved the microstructure. Optical microscopy revealed a reduction in the number of oxide inclusions and a transformation of their morphology from angular to semi-spherical. This morphological change indicates that the increased CaO activity enhanced the thermodynamic driving force for inclusion transformation. The calcium formed from the decomposition of $CaCO_3$ reacted with silicon oxide- and aluminum oxide-based inclusions, producing calcium silicate and calcium aluminate phases with low melting temperatures and low interfacial energies.

The observed inclusion modification is in good agreement with previous studies on refining slags. Zhan et al. [27] reported that the increase of slag basicity promotes the transformation of irregular oxide inclusions to calcium-bearing phases and decreases their average size. In addition, the studies on HSLA steels [26] revealed that high-basicity slags favor the formation of low-melting inclusions in the $CaO - MgO - Al_2O_3 - SiO_2$ system and, therefore, enhance the cleanliness of the steel by efficient flotation of inclusions into the slag phase. Therefore, the present results confirm that increasing the $CaCO_3$ content enhances the refining capability of the composite mineral flux.

The F3 flux (70 wt.% $CaCO_3$–30 wt.% $CaSiO_3$) produced the cleanest microstructure among all the investigated compositions. The large angular inclusions almost completely disappeared, and only a small number of fine spherical inclusions were uniformly distributed throughout the ferrite–pearlite matrix. It was found that the F3 composition provided the most favorable physicochemical conditions for inclusion modification during the remelting process.

The superior refining performance of the F3 slag is attributed to the optimum balance between slag basicity and fluidity. The basicity of the obtained slag was high enough to ensure the activity of CaO to form stable calcium silicate and calcium aluminate phases, but to preserve the necessary fluidity of the slag for effective flotation of inclusions. These results are in very good agreement with the thermodynamic calculations presented in this work. The negative values of Gibbs free energy indicate that the formation of calcium-containing phases occurs spontaneously under the experimental conditions.

These observations are also in good agreement with the industrial study reported by Xu et al. [28], who demonstrated that optimized refining slags significantly reduce the size and number density of inclusions in alloy steels. However, unlike the conventional calcium wire treatment used in secondary refining, the present study demonstrates that $CaCO_3 - CaSiO_3$ composite mineral fluxes can generate *in situ* active calcium through the decomposition of $CaCO_3$. This is particularly important as an alternative approach for inclusion modification during the remelting of recycled cast steel.

When the $CaCO_3$ content was increased to 80 wt.% (F4), the cleanliness of the steel deteriorated despite the higher slag basicity. Optical microscopy revealed numerous fine oxide particles and localized microporosity distributed throughout the steel matrix. These results indicate that excessive decomposition of $CaCO_3$ generated an excessive amount of CO_2, which increased the oxygen potential at the slag–metal interface and intensified secondary oxidation.

This observation differs from the widely accepted view that refining efficiency continuously improves with increasing slag basicity. However, the present study demonstrates that an excessive amount of $CaCO_3$ shifts the thermodynamic equilibrium back toward oxide formation. Such a relationship between oxygen potential and inclusion evolution has also been reported in previous thermodynamic studies [29,30]. However, no experimental confirmation of this phenomenon has previously been reported for recycled SCMnCr3 cast steel.

Overall, the optical metallographic observations demonstrate that steel cleanliness is governed not only by slag basicity but also by the combined effects of slag basicity, calcium activity, slag viscosity, and the kinetics of inclusion flotation. Because the F3 composition provides the optimum combination of these factors, it ensures the most effective modification and removal of non-metallic inclusions during the remelting process.

SEM, EDS, and elemental mapping analysis

The morphology of the microstructure formed after the remelting of SCMnCr3 steel using the F3 composite mineral flux (70 wt.% $CaCO_3$–30 wt.% $CaSiO_3$) was investigated by scanning electron microscopy (SEM) (**Fig. 4**). At higher magnifications, the steel matrix was characterized by a homogeneous ferrite–pearlite morphology containing only a small number of very fine secondary-phase particles. The large angular oxide inclusions that were widespread in the F1 and, to some extent, the F2 samples were almost absent in the F3 sample. Instead, the remaining inclusions were small, spherical, and uniformly distributed throughout the matrix, indicating that successful inclusion modification had been achieved during the remelting process.

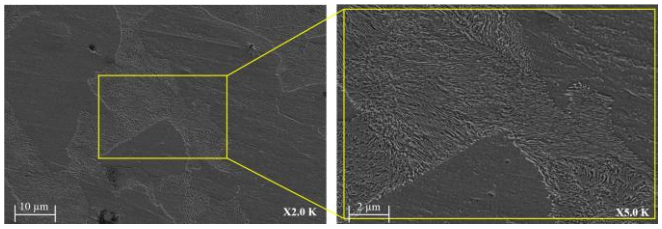

Fig. 4 SEM micrographs of the samples produced using the F3 flux

The absence of large and irregularly shaped particles indicates that the composite slag possessed sufficient refining capability and was able to transform the primary oxide inclusions into small calcium-containing compounds with low interfacial energy. The spherical morphology of the remaining inclusions is consistent with the occurrence of thermodynamically favorable modification processes under conditions of moderate slag basicity.

The analyzed region consisted predominantly of Fe, with high concentrations of Mn and Cr, while trace amounts of Si, Cu, and sulfur were also detected by energy-dispersive X-ray spectroscopy (EDS) (**Fig. 5**). The normalized elemental composition was approximately 42.75 wt.% Mn, 23.18 wt.% Cr, 21.78 wt.% C, 6.34 wt.% Si, 5.52 wt.% Cu, and only 0.43 wt.% S, whereas phosphorus was below the detection limit.

The low sulfur concentration indicates that the CaO-rich slag promoted desulfurization during the remelting process. Calcium oxide formed through the decomposition of $CaCO_3$ increases the sulfide capacity of the slag and promotes the transfer of sulfur from the molten steel into the slag phase. Consequently, only a very small amount of sulfur was detected in the investigated microstructure.

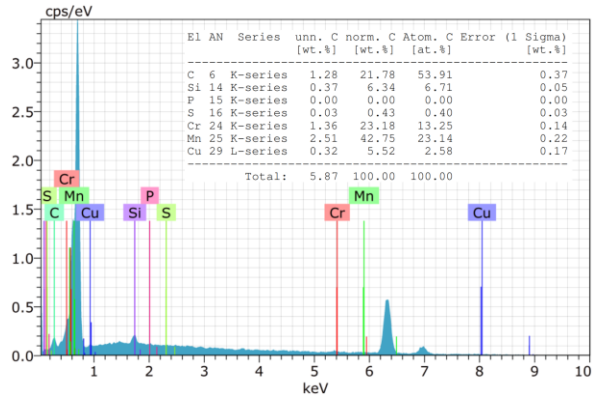

Fig. 5 EDS results of the samples produced using the F3 flux

The high contents of Mn and Cr are associated with the chemical composition of SCMnCr3 steel rather than with discrete oxide particles. These alloying elements were uniformly distributed and remained dissolved within the metal matrix, indicating that oxidation losses during remelting were successfully minimized by the optimized F3 slag composition.

Elemental mapping confirms this observation. No significant elemental segregation was observed and the spatial distribution of carbon, silicon, chromium, manganese and copper was generally uniform in the analyzed region. The iron map showed a continuous coverage over the matrix, suggesting that the microstructure seen was mainly consisting of the metallic phase without any significant presence of non-metallic inclusions. Very fine complex oxide or carbide particles have been observed possibly associated with localized enrichments of Mn and Cr. However, no continuous enrichment zones or clustered inclusions were detected, indicating that inclusion agglomeration during solidification was effectively prevented.

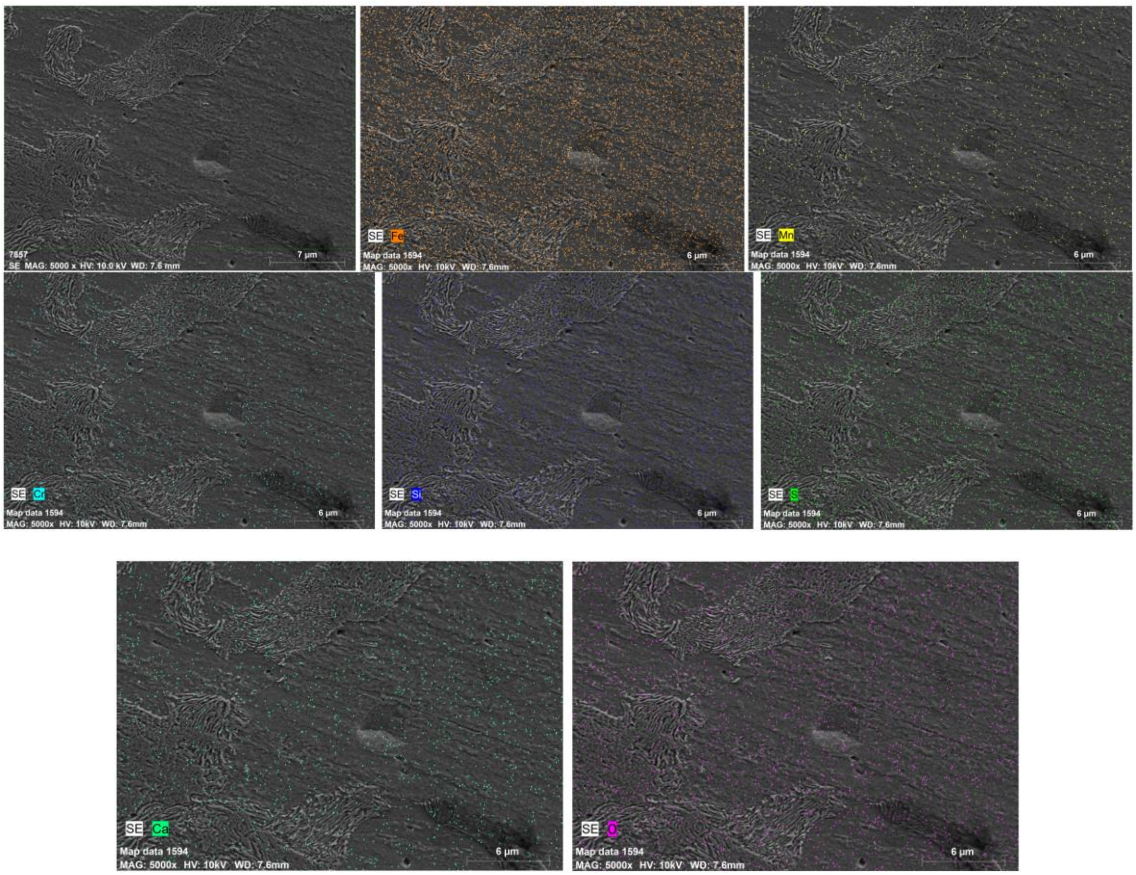

Fig. 5 Elemental mapping results of the samples produced using the F3 flux

The silicon map likewise exhibited an almost homogeneous distribution and the absence of silicon-rich oxide clusters. This result indicates that most of the silicon oxide formed during oxidation reacted with CaO before solidification to form calcium silicates. Such reactions reduce the amount of free SiO_2 and increase slag fluidity, thereby facilitating the flotation and removal of non-metallic inclusions.

The addition of calcium was effective, because calcium was enriched in the inclusions, while alloy elements were uniformly distributed in the steel matrix around the inclusions. Along the same lines, Tang et al. [23] reported that an effective refining can reduce the accumulation of oxide inclusions and improve the homogeneity of the elemental distribution. These findings are in full agreement with the observations of the present study.

The optimum slag basicity and slag fluidity contribute to the better microstructure of F3 sample from the thermodynamic point of view. The decomposition of about 70 wt.% $CaCO_3$ provides sufficient CaO to allow the formation of stable calcium silicates and calcium aluminates without producing excess CO_2 that may cause secondary oxidation. As a result, oxide inclusions are successfully transformed into fine particles with low interfacial energy and high flotation capability.

The present study demonstrates that the remelting of recycled cast steel using $CaCO_3 - CaSiO_3$ composite mineral fluxes can achieve a degree of inclusion modification comparable to that obtained by conventional calcium wire treatment. According to the proposed mechanism, calcium is generated in situ through the thermal decomposition of $CaCO_3$ and directly participates in slag–metal reactions without the need for an external calcium source. This refining approach represents a practical alternative for processing steel produced from metal scrap and simplifies the overall refining process.

X-ray diffraction (XRD) analysis

The crystal structure of the slag phases formed during the remelting of SCMnCr3 cast steel using $CaCO_3 - CaSiO_3$ composite fluxes with different compositions was determined by X-ray diffraction (XRD) analysis. Phase identification provides important information regarding slag chemistry, the mechanism of non-metallic inclusion modification, and the thermodynamic stability of oxide compounds.

The diffraction patterns showed that the composition of the slag phase changed systematically with increasing $CaCO_3$ content. These changes are closely associated with the decomposition of $CaCO_3$, the increase in CaO content, and the subsequent reaction of CaO with acidic oxides in the slag. The XRD results generally show that the formation of calcium-containing silicate and aluminate phases increases with increasing slag basicity and the amount of free silicon dioxide (SiO_2) decreases. However, too much $CaCO_3$ addition leads to formation of secondary oxide phases related to oxidation of iron, manganese and chromium.

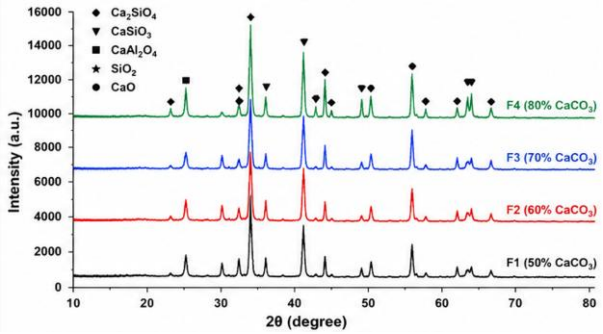

Fig. 6 XRD diffractograms of slag samples

For the F1 flux (50 wt.% $CaCO_3$–50 wt.% $CaSiO_3$), the diffraction pattern of the resulting slag was dominated by peaks corresponding to silica-rich phases. SiO_2 exhibited the highest-intensity diffraction peaks, while FeO produced additional reflections. The predominance of silicon dioxide indicates that the slag still possessed a strongly acidic character because the amount of CaO generated by the decomposition of $CaCO_3$ was insufficient to neutralize most of the free SiO_2.

The presence of FeO points out that only part of the oxide products formed during remelting has been transformed into calcium containing compounds. The oxide inclusions were thermodynamically stable in the steel matrix and did not change their composition. The XRD results are well consistent with metallographic observations, which showed many angular oxide inclusions in the ferrite–pearlite matrix.

F2 flux (60 wt.% $CaCO_3$–40 wt.% $CaSiO_3$). When the $CaCO_3$ content was increased to 60 wt.%, the diffraction pattern changed significantly. The intensity of the reflections corresponding to SiO_2 decreased, whereas new peaks associated with calcium silicate compounds became more pronounced.

Among all the investigated compositions, the F3 flux (70 wt.% $CaCO_3$–30 wt.% $CaSiO_3$) produced the most favorable phase composition. The strongest diffraction peaks corresponded to the $CaSiO_3$ and Ca_2SiO_4 phases, indicating that most of the silicon dioxide had reacted with CaO. In addition, several reflections characteristic of calcium aluminates were also detected, confirming the effective reaction of CaO with aluminum oxide inclusions. The presence of calcium silicates and calcium aluminates indicates a significant modification of non-metallic inclusions during remelting.

Cao et al. [30] also reported such phase transformations, combining thermodynamic equilibrium modelling to predict the evolution of oxides during steel refining. Their study also showed that higher calcium activity leads to stabilization of calcium-containing oxide phases, which is in full agreement with the experimental results of the present study.

Xu et al. [28] reached similar conclusions. They found that optimized refining slags significantly modify the chemical composition of inclusions and reduce their amount through the formation of stable calcium-rich compounds. Although their study was limited to industrial secondary refining, the present analysis demonstrates that similar phase evolution can also be achieved during the remelting of recycled SCMnCr3 cast steel using $CaCO_3 - CaSiO_3$ composite mineral fluxes.

One of the most important findings of the present study is that the F3 composition generated a sufficient amount of CaO to stabilize calcium silicate phases while maintaining the required slag fluidity. This composition provided optimum inclusion modification without excessive secondary oxidation. In contrast, the excessive $CaCO_3$ content in the F4 composition increased the oxygen content owing to intense CO_2 evolution and, consequently, reduced the overall refining efficiency despite the higher slag basicity.

Moreover, the severe evolution of CO_2 promotes the oxidation reactions and offers appropriate conditions for the formation of more FeO, MnO and Cr_2O_3 particles. Depending on the slag composition, these oxides may subsequently form complex mixed oxides, such as manganese chromite spinel or calcium-containing spinel phases [46–48].

The highest slag basicity resulted in an increased number of fine dispersed inclusions observed by optical microscopy, which is attributed to the presence of free CaO and secondary oxide phases.

Table 3 Phase evolution based on XRD analysis

Flux	Dominant crystalline phases	Interpretation
F1	SiO_2, FeO	Low basicity, limited inclusion modification
F2	$CaSiO_3$, $CaAl_2O_4$, residual SiO_2	Onset of calcium-induced inclusion modification
F3	$CaSiO_3$, Ca_2SiO_4, $CaAl_2O_4$	Optimum slag chemistry, effective refining
F4	$CaSiO_3$, Ca_2SiO_4, free CaO, FeO, traces of MnO / Cr_2O_3	Excessive basicity and secondary oxidation

Thermodynamic discussion

The experimental results obtained from optical metallography and X-ray diffraction (XRD) analyses were interpreted based on thermodynamic principles. During the remelting process, the evolution of non-metallic inclusions is governed by the thermodynamic equilibrium established among the molten steel, slag, and the surrounding environment. The principal factors controlling these reactions are slag basicity, the thermodynamic activity of oxides, oxygen potential, and Gibbs free energy.

During the remelting process, calcium carbonate decomposes according to the following reaction:

$$CaCO_3 \rightarrow CaO + CO_2 \quad (13.)$$

The resulting CaO is the principal basic oxide in the slag system. At the same time, the released CO_2 accelerates bath stirring and improves mass transfer between the slag and the molten steel. The increase in CaO concentration changes the chemical potential of the slag and shifts the equilibrium toward the formation of stable calcium-containing compounds.

Effect of slag basicity. According to the calculations, the slag basicity increased progressively with increasing $CaCO_3$ content.

Table 4 Dependence of slag basicity on flux composition

Flux	F1	F2	F3	F4
Basicity (B)	1.20	1.60	1.80	2.30

The increase in slag basicity directly enhanced the thermodynamic tendency of CaO to react with acidic oxides in the slag. The principal reaction responsible for the removal of silicon dioxide is:

$$CaO + SiO_2 \rightarrow CaSiO_3 \quad (14.)$$

Since the Gibbs free energy of this reaction is negative within the investigated temperature range of 1550–1600 ℃, the formation of calcium silicate occurs spontaneously. The XRD results, which showed a reduction in the amount of free SiO_2, confirm these thermodynamic calculations.

Thermodynamic activity of CaO. Although slag basicity is an important macroscopic parameter, the actual refining efficiency depends on the thermodynamic activity of CaO.

The activity is determined by the following equation:

$$a_{CaO} = \gamma_{CaO} X_{CaO} \quad (15.)$$

where: X_{CaO} – the mole fraction of CaO;
γ_{CaO} – the activity coefficient.

The calculated values showed that the activity of CaO increased continuously with increasing $CaCO_3$ content.

Table 5 Dependence of CaO activity on flux composition

Flux	F1	F2	F3	F4
CaO activity	0.35	0.55	0.74	0.90

An increase in CaO activity enhances the thermodynamic driving force for inclusion modification. However, excessively high activity leads to the formation of free CaO and reduces slag stability.

At steelmaking temperatures, the Gibbs free energy is negative for Reactions (8), (9), and (10). Therefore, the formation of calcium silicate, calcium aluminate, and calcium sulfide is thermodynamically favorable. These reactions occur

spontaneously. Consequently, calcium-based compounds provide high efficiency in removing oxygen, sulfur, and non-metallic inclusions from the molten metal.

Oxidation of chromium and manganese. Unlike plain carbon steels, SCMnCr3 contains chromium and manganese, which actively participate in oxidation reactions.

Oxidation of chromium: $4Cr + 3O_2 \rightarrow 2Cr_2O_3$ (16.)

Oxidation of manganese: $2Mn + O_2 \rightarrow 2MnO$ (17.)

Chromium and manganese oxides are thermodynamically relatively stable.

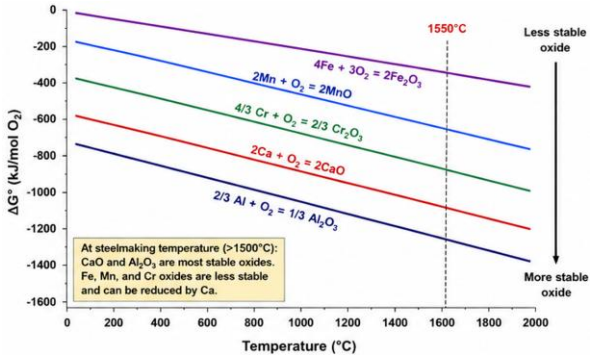

Fig. 7 Ellingham diagram

The Ellingham diagram shows that the Gibbs free energy of Cr_2O_3 is lower than that of FeO. Therefore, under the same oxygen potential, chromium is oxidized preferentially to iron.

The resulting Cr_2O_3 particles may subsequently form more stable calcium chromite phases through the following reaction:

$$CaO + Cr_2O_3 \rightarrow CaO \cdot Cr_2O_3 \quad (18.)$$

Similarly,

$$CaO + MnO \rightarrow CaO \cdot MnO \quad (19.)$$

the above reaction may also occur depending on the slag composition. These reactions explain the inclusion modification observed in the F2 and F3 samples.

Secondary oxidation. The highest slag basicity was observed for the F4 composition. However, optical microscopy revealed an increase in the number of oxide inclusions. This phenomenon is explained by secondary oxidation.

The large amount of CO_2 generated by the decomposition of $CaCO_3$ makes the following reaction thermodynamically favorable:

$$Fe + CO_2 \rightarrow FeO + CO \quad (20.)$$

The resulting FeO reacts with the alloying elements in the molten steel, forming new secondary oxide inclusions. Therefore, higher slag basicity does not always imply cleaner steel. Instead, an optimum balance among the thermodynamic activity of CaO, oxygen potential, and slag viscosity must be achieved.

Relationship between CaO activity and inclusion density. The experimental results demonstrate an inverse relationship between CaO activity and inclusion density up to the optimum slag composition. As the activity increases from F1 to F2 to F3, the number of inclusions decreases. However, in the F4 composition, the activity increase further enhances the secondary oxidation, and the inclusion density increases. This the relation is not linear but parabolic. As the CaO activity increases from 0.35 to 0.74, the inclusion density decreases. Beyond this value, the number of inclusions increases again because of secondary oxidation and excessive gas evolution.

The formation of calcium silicate becomes thermodynamically more stable with increasing temperature. Within the investigated temperature range of 1550–1600 ℃, the Gibbs free energy remains negative. Therefore, the reaction $CaO + SiO_2 \rightarrow CaSiO_3$ occurs spontaneously throughout the entire temperature range.

Chemical composition of the research samples after flux treatment

The chemical composition of the SCMnCr3 steel after treatment with the investigated $CaCO_3 - CaSiO_3$ fluxes was determined by optical emission spectrometry. Three independent samples were analyzed for each flux condition (n = 3), and the results are presented as mean ± standard deviation in Table 6.

Table 6. Chemical composition of SCMnCr3 steel after treatment with different $CaCO_3 - CaSiO_3$ fluxes (mean ± SD, n = 3).

Flux	C	P	S	Mn	Si	Cr	Ni	Cu	Al
F1	0.418	0.033	0.0283	1.153	0.973	0.800	0.107	0.150	0.205
F2	0.415	0.033	0.0267	1.150	1.013	0.820	0.143	0.143	0.205
F3	0.421	0.033	0.0207	1.280	0.940	0.977	0.073	0.130	0.0357
F4	0.420	0.031	0.0270	1.180	0.833	0.847	0.077	0.133	0.0737

The results demonstrate that the chemical composition of the steel varied depending on the flux composition. The most significant change was in the sulfur content. The mean sulfur content was reduced from 0.026 wt.% in the original SCMnCr3 steel to 0.0207 ± 0.0015 wt.% after treatment with the F3 flux, which corresponds to a relative reduction of about 20.5 %. The average sulfur contents after F1, F2 and F4 treatments are 0.0283 ± 0.0051, 0.0267 ± 0.0045 and 0.0270 ± 0.0010 wt.%, respectively, as a reference.

The mean Mn concentration was also 1.280 ± 0.035 wt.% and the Cr concentration was 0.977 ± 0.012 wt.% for the F3 treatment. The corresponding Cr concentrations for F1, F2, and F4 were 0.800 ± 0.052, 0.820 ± 0.085, and 0.847 ± 0.038 wt.%, respectively. Since the measured bulk chemical composition can be affected by the initial compositional variation and experimental conditions, the differences in Mn and Cr concentrations are not interpreted solely as evidence of elemental oxidation or loss.

Evolution mechanism of non-metallic inclusions

The evolution mechanism of non-metallic inclusions during the remelting of SCMnCr3 cast steel is comprehensively explained based on optical metallography, X-ray diffraction (XRD) analysis, and thermodynamic calculations.

Unlike plain carbon steels, SCMnCr3 steel contains chromium, manganese, and silicon, which actively participate in the oxidation and modification processes of inclusions. Therefore, the formation of non-metallic inclusions depends not only on slag basicity but also on oxygen potential, the thermodynamic activity of oxides, and the thermodynamic stability of the oxides of alloying elements.

The mechanism proposed in the present study consists of a sequence of physicochemical stages.

According to the proposed theory, the evolution of non-metallic inclusions during the remelting process is governed by the competition between two thermodynamic processes.

The first process is calcium-induced modification, which transforms angular oxide inclusions into spherical, calcium-rich compounds that are readily absorbed by the slag.

The second process is secondary oxidation caused by excessive CO_2 evolution, which leads to the continuous formation of new oxide particles.

The optimum flux composition is the one that provides a balance between these two opposing mechanisms.

For the investigated SCMnCr3 cast steel, this balance was achieved with the composite mineral flux containing 70 wt.% $CaCO_3$ and 30 wt.% $CaSiO_3$. This composition provided the maximum effective slag basicity without intensifying excessive oxidation.

Under these conditions, the steel exhibited the lowest inclusion density, the most favorable spherical inclusion morphology, and the cleanest microstructure.

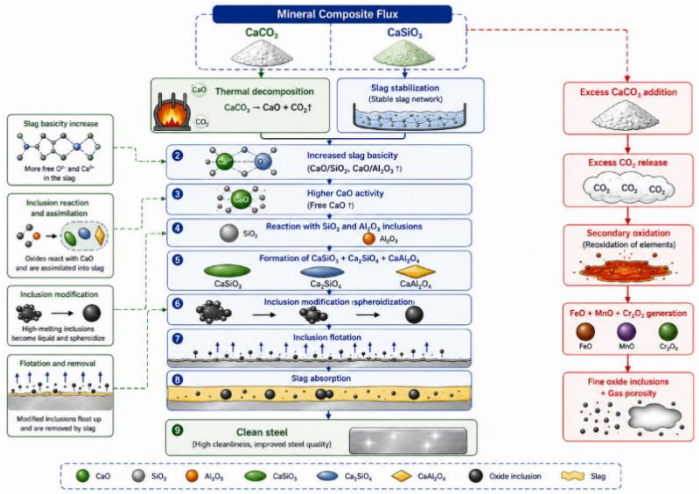

Fig. 8 Schematic illustration of the proposed evolution mechanism of non-metallic inclusions in alloy

CONCLUSION

The effect of $CaCO_3 - CaSiO_3$ composite mineral fluxes on the evolution of non-metallic inclusions during the remelting of recycled SCMnCr3 cast steel was comprehensively investigated through the combined application of experimental characterization techniques and thermodynamic analysis. In summary, the main conclusions are as follows:

The composition of the $CaCO_3 - CaSiO_3$ composite flux greatly influenced the slag basicity, inclusion evolution and cleanliness of the remelted steel. Increasing $CaCO_3$ content promoted the formation of CaO, which enhanced the refining ability of the slag and facilitated the modification of oxide inclusions.

The results of SEM, EDS, elemental mapping, XRD analysis and optical microscopy showed that the flux with 70 wt.% $CaCO_3$ and 30 wt.% $CaSiO_3$ (F3) resulted in the cleanest microstructure. This composition can effectively reduce the amount of large and irregular oxide inclusions, and promote the formation of fine and uniformly distributed spherical inclusions. These results indicated successful inclusion modification during the remelting process.

The thermodynamic analysis showed that the decomposition of $CaCO_3$ increased the activity of CaO and therefore promoted the formation of thermodynamically stable calcium silicate and calcium aluminate phases. These reactions decreased the interfacial energy of the inclusions, favoured their flotation into the slag phase and improved the cleanliness of the steel.

The presence of excess $CaCO_3$ beyond the optimum level (80 wt.%) led to excessive CO_2 evolution during decomposition. The increased oxygen potential promoted the formation of more oxide inclusions and enhanced the secondary oxidation. Thus, the slag basicity was increased but the overall refining efficiency was decreased.

The results indicate that the optimal balance between slag basicity and slag fluidity is more important than simply maximizing slag basicity. The F3 composite flux provided the most favourable physicochemical conditions for modifying the inclusions, promoting interaction between the slag and the metal, and removing the inclusions during remelting.

Acknowledgements: The authors express their deep gratitude to JSC "Uzmetkombinat" production enterprise for its support in carrying out the experimental work.

REFERENCES

1. M.A. Guitar, A. Thome, D. Britz: Discover Sustainability, 6(1), 2025, 405. https://doi.org/10.1007/s43621-025-01254-1
2. C. Wang, S.D.C. Walsh, Z. Weng, M.W. Haynes, D. Summerfield, A. Feitz: International Journal of Hydrogen Energy, *48*(83), 2023, 32277-32293. https://doi.org/10.1016/j.ijhydene.2023.05.041
3. S.G. Saveliev, et al.: Progress in Physics of Metals, 26(2), 2025, 427–441. https://doi.org/10.15407/ufm.26.02.427
4. X. Yao, H. Xie: Processes, 12(2), 2024, 340. https://doi.org/10.3390/pr12020340
5. N. Kholmirzaev, et al.: Acta Metallurgica Slovaca, 32(2), 2026, 116–123. https://doi.org/10.36547/ams.32.2.2284
6. A. Peela, A. Mikitisin, F. Steinweg, T. Janitzky, A. Schwedt, C. Broeckmann, J. Mayer: Wear, 566–567, 2025, 205767. https://doi.org/10.1016/j.wear.2025.205767
7. R. Musi, M. Schickbichler, M. Burtscher, S.K. Michelic, K. Thiele: ISIJ International, 65(13), 2025, 2213-2225. https://doi.org/10.2355/isijinternational.ISIJINT-2025-260
8. N. Kholmirzaev, et al.: Materials Science Forum, 1139, 2024, 3-9. https://doi.org/10.4028/p-2AMBsZ
9. N. Saidmakhamadov, et al.: AIP Conference Proceedings, 3268(1), 2025, 030002. https://doi.org/10.1063/5.0257618
10. N. Kholmirzaev, et al.: E3S Web of Conferences, 525, 2024, 03012. https://doi.org/10.1051/e3sconf/202452503012
11. N. Saidmakhamadov, et al.: AIP Conference Proceedings, 3390(1), 2026, 080011. https://doi.org/10.1063/5.0321874
12. J. Campbell: Steel Research International, 88(1), 2017, 1600093. https://doi.org/10.1002/srin.201600093
13. C. Shi, V. Schulze, S. Dietrich: Materials Science and Technology, 40(2), 2024, 107-119. https://doi.org/10.1177/02670836231212614
14. J. Wang, B. Guo, B. Lyu, L. Zhang: Journal of Materials Research and Technology, 32, 2024, 1761-1771. https://doi.org/10.1016/j.jmrt.2024.08.005
15. F.A. Calderon Hurtado, J. Govro, A. Emdadi, R.J. O'Malley: Metals, 14(7), 2024, 821. https://doi.org/10.3390/met14070821
16. J.D. Steenkamp, L. du Preez: Journal of the Southern African Institute of Mining and Metallurgy, 115(6), 2015, 557-561.
17. Y. Sahai: Metallurgical and Materials Transactions B: Process Metallurgy and Materials Processing Science, 47(4), 2016, 2095–2106. https://doi.org/10.1007/s11663-016-0648-3
18. J.H. Park, Y.B. Kang: Steel Research International, 95(11), 2024, 2300598. https://doi.org/10.1002/srin.202300598
19. T.T. Zhang, J. Ding, B.Y. Ma, Z.L. Liu, C. Yu, C.J. Deng: Journal of Iron and Steel Research International, 31(6), 2024, 1291–1303. https://doi.org/10.1007/s42243-024-01191-9
20. Y. Ren, W. Wang, W. Yang, L. Zhang: ISIJ International, 63(12), 2023, 1927-1940. https://doi.org/10.2355/isijinternational.ISIJINT-2023-143
21. S.K. Michelic, C. Bernhard: Steel Research International, 93(7), 2022, 2200086. https://doi.org/10.1002/srin.202200086
22. Z. Zhan, et al.: Metals, 13(4), 2023, 750. https://doi.org/10.3390/met13040750
23. T. Hai-Yan, et al.: Origin and Evolution of Non-Metallic Inclusions For Al-Killed Steel During Eaf-Lf-Vd-Cc Process. In *7th International Symposium on High-Temperature Metallurgical Processing*, Hoboken, NJ, USA: John Wiley & Sons, Inc., 2016, pp. 271-278. https://doi.org/10.1002/9781119274643.ch34

24. Z. Deng, M. Zhu: Formation and Evolution of Spinel Inclusions during Al-Killed Steel Refining. In *Proceedings of the 8th Pacific Rim International Congress on Advanced Materials and Processing*, Cham: Springer International Publishing, 2013, pp. 753-760. https://doi.org/10.1002/9781118792148.ch93
25. Z. Deng, M. Zhu: ISIJ International, 53(3), 2013, 450-458. https://doi.org/10.2355/isijinternational.53.450
26. H. Yu, X. Wang, J. Zhang, W. Wang: High Temperature Materials and Processes, 34(7), 2015, 675-682. https://doi.org/10.1515/htmp-2014-0116
27. N. Saidmakhamadov, et al.: AIP Conference Proceedings, 3390(1), 2026, 020014. https://doi.org/10.1063/5.0322231
28. G. Xu, et al.: Journal of Materials Research and Technology, 34, 2025, 209-219. https://doi.org/10.1016/j.jmrt.2024.12.060
29. J. Cao, et al.: Crystals, 13(2), 2023, 202. https://doi.org/10.3390/cryst13020202
30. L. Cao, L. Zhu, R. Zhao, Z. Guo, G. Qiu: Metals, 13(10), 2023, 1680. https://doi.org/10.3390/met13101680
31. X. Lu, et al.: Metals, 12(5), 2022, 718. https://doi.org/10.3390/met12050718
32. M. Schickbichler, J. Cejka, S. Michelic: Metallurgical and Materials Transactions B, 57, 2026, 3809–25. https://doi.org/10.1007/s11663-026-04074-4
33. P. S. Minh, V.T. Nguyen, T. Nguyen, V.T. Nguyen, N. Ho: Acta Metallurgica Slovaca, 31(3), 2025, 171–180. https://doi.org/10.36547/ams.31.3.2220
34. S.K. Arinova, V.Y. Kulikov, S.S. Kvon, A.E. Altynova: Acta Metallurgica Slovaca, 31(2), 2025, 74-77. https://doi.org/10.36547/ams.31.2.2153
35. T.S. Kim, G.H. Park, D.W. Kim, J.H. Park: Steel Research International, 96(8), 2025, 2400491. https://doi.org/10.1002/srin.202400491
36. Y. Zhang, Y. Ren, L. Zhang: *Metallurgia Italiana*, *111*(3), 2019, 25-34.
37. M. Harris: Evolution of non-metallic inclusions in foundry steel casting processes processes. In *Proceedings of the 69th Annual Technical and Operating Conference, Steel Founders Society of America (SFSA)(2015, Chicago Illinois), Steel Founders society of America (SFSA)(Dec 2015)*.
38. S. Duan, T. Kim, J. Cho, J.H. Park: Journal of Materials Research and Technology, 24, 2023, 5165-5176. https://doi.org/10.1016/j.jmrt.2023.04.115
39. S. Khasanov, U. Mardonov, A. Ongboyev, M. Ismatov: International Journal of Mechatronics and Applied Mechanics, 2024(16), 2024, 163-170. https://doi.org/10.17683/ijomam/issue16.19
40. U. Mardonov, et al.: International Journal of Mechatronics and Applied Mechanics, 2(22), 2025, 213-223. https://doi.org/10.17683/ijomam/issue22.v2.22
41. U. Mardonov, S. Madaminov, A. Jeltukhin, Y. Meliboev: Journal of Engineering and Technological Sciences, 58(2), 2026, 217–226. https://doi.org/10.5614/j.eng.technol.sci.2026.58.2.5
42. J. Isaksson, et al.: Metallurgical and Materials Transactions B: Process Metallurgy and Materials Processing Science, 56(3), 2025, 2573–2586. https://doi.org/10.1007/s11663-025-03510-1
43. S. Tursunbayev, et al.: E3S Web of Conferences, 390, 2023, 05046. https://doi.org/10.1051/e3sconf/202339005046
44. S. Tursunbaev, et al.: E3S Web of Conferences, 401, 2023, 05001. https://doi.org/10.1051/e3sconf/202340105001
45. X. Li, et al.: Journal of Magnesium and Alloys, 16, 2025, 101812. https://doi.org/10.1016/j.jma.2025.06.029
46. J.B. Chen, H.H. Huang, R. Chu, Y.Q. Sun: ISIJ International, 61(6), 2021, 1842-1849. https://doi.org/10.2355/isijinternational.ISIJINT-2020-730
47. S.J. Kim, et al.: ISIJ International, 53(8), 2013, 1325-1333. https://doi.org/10.2355/isijinternational.53.1325
48. A. Slagter, et al.: Metallurgical and Materials Transactions A: Physical Metallurgy and Materials Science, 55(5), 2024, 1469–1483. https://doi.org/10.1007/s11661-024-07330-x